**Light Metals 2012** *Edited by: Carlos E. Suarez*
***TMS (The Minerals, Metals & Materials Society), 2012***

# FRICTION STIR WELDING OF Al- Zn- Mg ALLOY AA7039

Chaitanya Sharma, D. K. Dwivedi*, P. Kumar,
Mechanical and Industrial Engineering Department,
I.I.T., Roorkee, Uttarkhand, India-247667
*Corresponding author: e-mail:dkd04fme@iitr.ernet.in
Tel.: 91-1332-285826, Fax: 91-1332 -285665.

Keywords: Friction stir welding, microstructure, mechanical and corrosion properties

## Abstract

In this investigation Al-Zn-Mg alloy AA7039 was friction stir welded (FSW) successfully employing a rotary speed of 635 rpm and welding speed of 75 mm/min, in order to elucidate the effect of FSW on mechanical and corrosion properties. The yield and ultimate tensile strength of the joint were found lower than the base material while ductility of FSW joint was found higher than the base material. The joint efficiency of friction stir welded joint was 85.59 %. The microstructure and other unique features associated with different zones of FSW joints were studied by optical and scanning electron microscopy. SEM study of fracture surfaces revealed that fracture is triggered by the breaking of secondary precipitates ($MgZn_2$). Weld nugget of FSW joint was found to be susceptible to corrosion than HAZ and base metal. The current density for WNZ and HAZ were ~8.5 and 2.8 times higher than that of the base metal.

## 1. Introduction

The fusion welding of precipitation hardening aluminum alloys results in loss of strength of heat affected zone because of coarsening of α-Al grains and dissolution of strengthening precipitates and other fusion welding related problems [1]. This kind of loss of strength can be minimized by controlling heat input to the weld or using other joining process. FSW has been reported to reduce problems related with fusion welding as maximum temperature (~ 425- 480$^0$c) observed during FSW is significantly lower than the melting temperature of aluminum alloys [2]. FSW of difficult to weld materials offers many advantages such as better joint properties and fatigue lives, low energy consumption, no harmful emission, high level of dimension stability and repeatability. These advantages make FSW an ideal choice for joining aluminum alloys for transportation, rail, marine and aerospace applications [3].

AA7039 is a medium strength alloy based on Al-Zn-Mg system of 7XXX series alloys which gains strength from $MgZn_2$ precipitation and can be fusion welded with few difficulties arising from the melting and solidification. This alloy is highly suited for military and other structural applications where on site repair and maintenance work is required [4].

Aluminum alloys generally possess good corrosion resistance due to the formation of protective oxide layer, however they show tendency to localized corrosion when exposed to harsh environments. Differential thermal and mechanical stresses experienced by the base metal during FSW results in the formation of various zones exhibiting varying microstructural characteristics. Therefore, it is expected that different FSW zones will exhibit different responses to corrosion. Further, susceptibility to corrosion increases with the sanitization (depletion of precipitate) of the weld microstructure of FSW joints of high strength 2xxx and 7xxx series aluminum alloys [5, 6].

Many research papers are available in the literature on various aspects of friction stir welded aluminum alloys such as material flow, development of microstructure and mechanical properties, effect of process parameters, fatigue and corrosion behaviour [7-13]. Literature review reveals that not much information are available in open literature on the mechanical and corrosion behaviour of AA7039 [14,15] therefore, in this present study AA7039 Al alloy was friction stir welded to experimentally examine the effect of FSW on microstructure, mechanical and corrosion properties of the developed joints.

## 2. Experimental methods

The chemical composition and mechanical properties of AA 7039 base metal, 5 mm thick extruded plates are given in Tables 1.

**Table 1: Chemical composition and mechanical properties of AA 7039 aluminium alloy**

| Chemical composition (wt%) | | | | | | | Mechanical properties | | | |
|---|---|---|---|---|---|---|---|---|---|---|
| Al | Zn | Mg | Mn | Fe | Si | Cu | Ultimate tensile strength (MPa) | Yield strength (MPa) | Elongation (%) | Microhardnes (Hv) |
| Bal. | 4.69 | 2.37 | 0.68 | 0.69 | 0.31 | 0.05 | 414 | 328 | 15.1 | 135 |

Friction stir welding of AA7039 plates of size 300 X 50 X 5 mm$^3$ was performed parallel to plate extrusion direction on modified vertical milling machine (HMT India, 7 H.P. and 635 rpm). The welding and tool geometry parameters used for the production of weld joints are enlisted in Table 2. FSW tool was made of die steel and had flat shoulder with truncated conical pin having anticlockwise thread of 1mm pitch.

**Table 2: Tool dimension and welding parameters used for friction stir welding of AA 7039 aluminium alloy**

| Tool dimensions | | | | Welding parameters | | |
|---|---|---|---|---|---|---|
| Shoulder diameter (mm) | Pin diameter (mm) Top | Bottom | Pin length (mm) | Welding speed (mm/min) | Rotary speed (rpm) | Tool tilt (degrees) |
| 16 | 6 | 4 | 4.7 | 75 | 635 | 2.5 |

Weld joints were inspected visually for voids, cracks and other surface defects. Thereafter, FSW joints were subjected to three point bend test to reveal the presence of subsurface defects. FSW joints passed 90$^0$ face and root bend test and no crack was observed on external surface subjected to bending. Electro-mechanically controlled UTM (H25K-S, Hounsfield) was used for conducting tensile tests in triplicate using specimens prepared according to ASTM E8M guidelines [16]. A Vickers microhardness tester (VHM-002V Walter UHL, Germany) was used for measuring the variation of hardness across the joint with a load of 1 N and 30 s dwell time.

Microstructure of FSW joints etched in Keller's reagent was observed using a light optical microscope (Leica, Germany). Average grain sizes of α Al present in base metal and different zones of FSW joints were determined using Image J, image analyzing software. The fracture surfaces of the tensile tested specimens were investigated by a FE-SEM (FEI-Quanta 200®). Prior to immersion corrosion test, the specimens were grounded to 1000 grit SiC paper finish, cleaned with ultra-sonic cleaner using distilled water as a medium and dried in air. A flat corrosion cell was used with three electrodes: test sample of 1 $cm^2$ exposed area, Ag/AgCl saturated KCl reference electrode and platinum wired counter-electrode. Scan rates were applied to the cell with the use of PARSTAT 2273 ®, operated by the software PowerSuite®. The surface roughness values before and after immersion in 3.5% NaCl solution, is measured by a Wyko NT 1100 optical profilometer interfaced with Vision [R]32 software.

### 3. Microstructure

Severe plastic deformation and heat generation during friction stir welding results in the formation of weld nugget zone (WNZ), thermo mechanically affected zone (TMAZ), and heat affected zone (HAZ) in the base metal, which are characteristic to FSW as shown in Fig.1a.

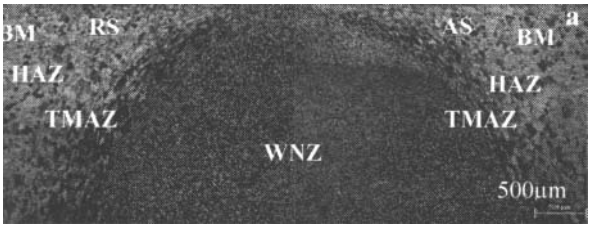


The weld nugget showed fully recrystallized finer equiaxed grains of α-Al (average size 13.12 μm) than base metal (44.3 μm) (Fig.1b). The coarse second phase strengthening precipitates ($MgZn_2$) present in the base metal could not be seen in the WNZ.

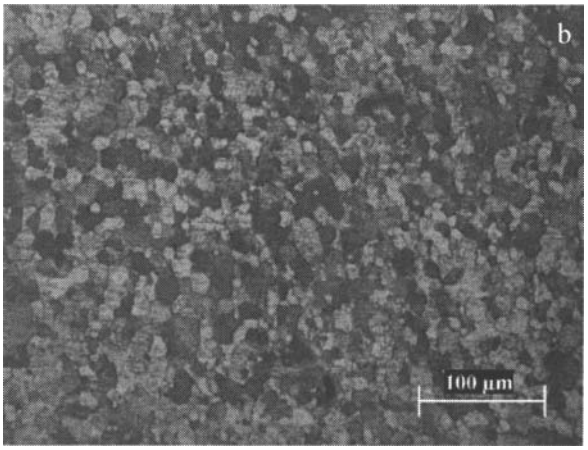


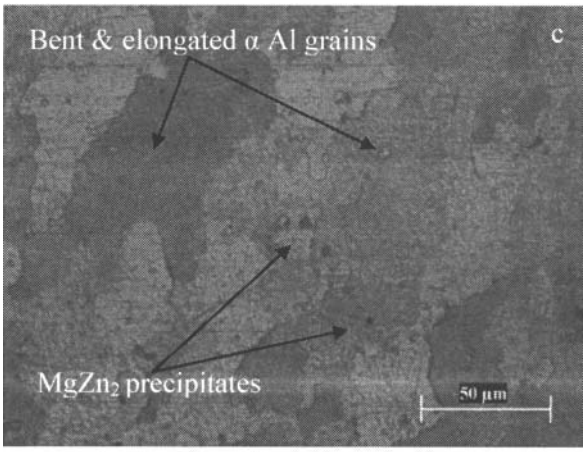


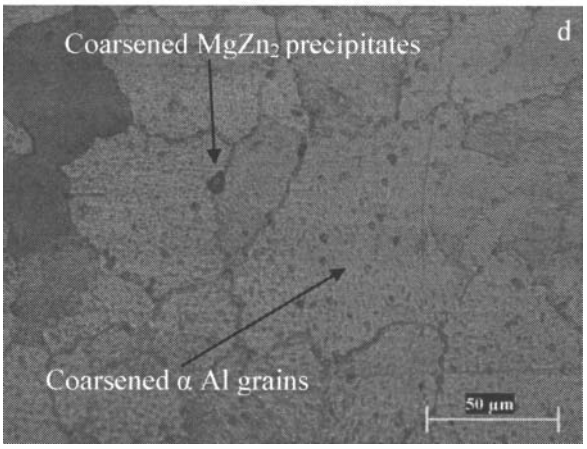


**Fig.1: Microstructure evolution in friction stir welded joint of AA7039, (a) Different FSW zones, (b) Fine recrystallized grains in WNZ, (c) Bent elongated grains in TMAZ, and (d) Coarsened grains in HAZ.**

These structural changes can be attributed to a) breaking and uniform distribution of second phase particles in the WNZ by stirring action of rotating and traversing tool and b) their dissolution in to α aluminium matrix as temperature rise in weld nugget zone is found to be greater than $400^0$C at which solutionizing can take place. WNZ had inverted trapezoidal shape whose length at top and bottom are 16.57 mm and 4.24 mm respectively. TMAZ is adjacent to WNZ and had elongated non recrystallized grains of average width 37.33-53.47 μm (Fig.1c). The TMAZ showed elongated and distorted grains without recrystallization. The WNZ and TMAZ interface was found to be clearer on advancing side (AS) than retreating side (RS) (Fig.1a) due to the fact that higher plastic strains and shear flow stresses are experienced by the material in narrow band on advancing side than retreating side arising from differences in relative velocity of tool with respect to workpiece in two sides [17]. Grain structure of HAZ was similar to base metal except that α aluminium grains were significantly coarsened (75.67 μm) because of dissolution of fine strengthening precipitate (Fig.1d).

### 4. Mechanical Properties

Transverse tensile tests were performed to determine tensile properties of FSW joint. Table 3 represents the average tensile properties of friction stir welds as well as base metal. FSW joints showed higher ductility (% elongation) and lower tensile strength than base metal (Refer table 3). The ductility of FSW joints (21.4%) was found significantly higher than base metal (15.1%) which also resulted in increased energy (23.8%) absorbed up to fracture. Yield (217.3 MPa) and ultimate tensile strength (354.4 MPa) of FSW joints were lower than the base metal and the same may be attributed to the dissolution/overaging of strengthening precipitates in WNZ/HAZ of FSW Joints. Joint strength efficiency (the ratio of weld strength to base metal strength) and elongation efficiency (ratio of % elongation of weld to that of base metal) [18] of FSW joints of AA7039 aluminum alloy were 85.6% and 141.7 % respectively. The average microhardness in the WNZ of FSW joint was 116 Hv respectively. The microhardness of weld nugget was significantly lower than base metal. The microhardness maxima (139 Hv) and minima (89 Hv) of FSW joint were found in TMAZ and HAZ on retreating (~3.5mm from weld centre) and advancing side (~6 mm from weld centre) respectively. During tensile testing the samples fractured from minimum hardness region of HAZ having lower tensile strength on AS along a path inclined at $45^0$ to the axis of loading and same is attributed to overaging of fine strengthening precipitates in HAZ [1].

## 5. Fractography

SEM fractographs of fractured surfaces of tensile specimens of base metal and FSW joints are shown in Fig. 2. Base metal had undergone transgranular ductile fracture and fracture surface covered with fine dimples of varying size and shapes (Fig. 2a).

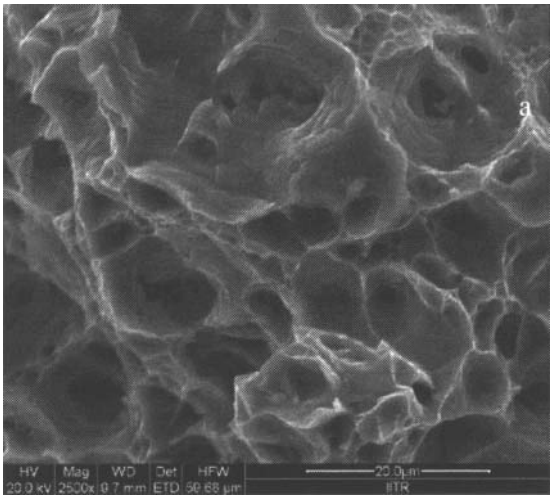


Some deep voids and enlarged dimples were also observed on the fracture surface. Fractured surfaces of welded joints invariably showed dimples of varying size and shape (Fig. 2b), which indicates that fracture is mostly ductile in nature. Voids on fracture surface of FSW joints contained secondary precipitates in considerable amount while base metal did not show any. Fracture originated from the breakages of secondary precipitates rich in Mg and Zn which initiated the formation of micro voids at grain boundary particles and coalesce at failure.

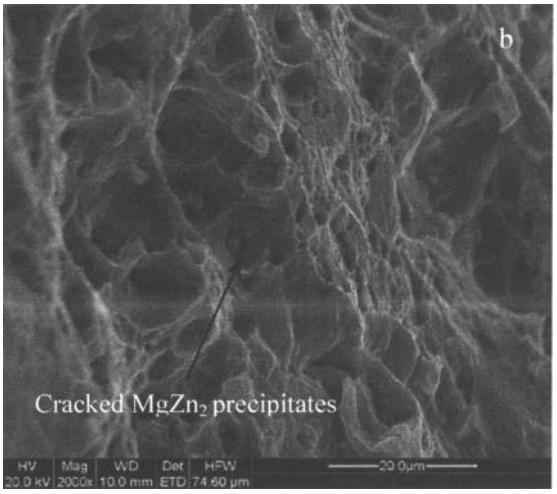


**Fig.2: Fracture surfaces, (a) Base metal, and (b) FSW joint of AA7039**

## 6. Corrosion Properties

The corrosion potential ($E_{corr}$), or open circuit potential (OCP), is an unique mixed potential at which rates of anodic and cathodic reaction are exactly same and equals the corrosion rate [19]. OCP variation of base metal, WNZ and HAZ, after immersion in 3.5% NaCl solution showed a maximum value of -920, -953 and -943 mV respectively (Fig.3). The potential of base metal and HAZ gradually shifted in the negative direction while that in case of WNZ it first shifted in positive direction for first 100 seconds, afterward it abruptly decreases for next 400 seconds. All (base metal, weld nugget and HAZ) after immersion of 1200 seconds followed similar trend and became stabilized after approximately1 hour of immersion. The potential of base metal, WNZ and HAZ were 931, 954 and 957 mV respectively at the end of immersion test. The base metal showed lower OCP than WNZ and HAZ suggesting that WNZ and HAZ are more prone to corrosion than base metal.

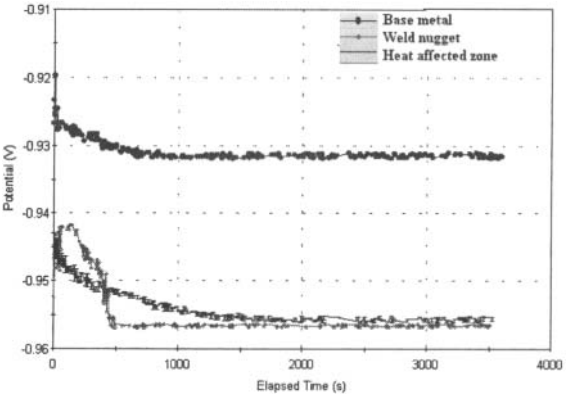


**Fig.3: Open circuit potential variation in 3.5% NaCl solution**

Potentiodynamic polarization curves for Tafel analysis of base metal, WNZ and HAZ in 3.5% NaCl solution are shown in Fig.4.

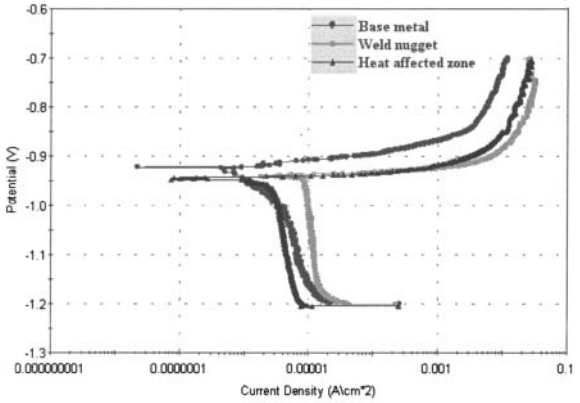


**Fig.4: Potentiodynamic polarization curves for Tafel analysis in 3.5% NaCl solution**

The results of Tafel analysis along with OCP after an immersion of 1hour in 3.5% NaCl solution are listed in table 4. It was found that initially current density increased aburptly with slight increase in corrosion potential followed by gradual increase with rapid increase in corrosion potential. These suggest that occurance of repassivation due to the formation of passive oxide film which was broken/absent intially because aggressive $Cl^-$ ions prevents the formation of passive oxide film[20].

The corrosion potential ($E_{corr}$) and current density ($I_{corr}$) for WNZ and HAZ were found higher than base material. The current density for WNZ and HAZ were ~8.5 and 2.8 times higher than that of the base metal indicating the lower corrosion resistance of weld nugget and HAZ as as high current density suggests higher corrosion rate. The main strengthening precipitate in Al-Zn-Mg alloy AA7039 is $MgZn_2$. The $\eta$ phase strengthening precipitate are found both in $\alpha$ aluminum matrix and at grain boundaries. These $\eta$ pahse precipitates were dissolved in WNZ and coarsened at grain boundary in FSW joint depending upon FSW parameters [1]. The WNZ had refined grain structure and different pecipitate distribution than base metal. The senitization (owing to thermal effects) leads to the depletion of Zn and formation of solute free zones. These precipitates free zones (PFZs) are found to be more reactive than $\alpha$ aluminum matrix resulting in increased anodic reactivity of the WNZ and HAZ than base metal. Thus making WNZ more sucesspetible to corrosion [21]. Since grain structure in HAZ is simillar to base metal except coarse precipitates and few PFZs along subgrain boundaries [6]. Hence, corrosion sucesspetibility of HAZ is found lower than WNZ. Images of corroded surfaces of base metal and WNZ after immersion corrosion test in 3.5% NaCl solution are shown in Fig.5. Base metal showed many tiny pits while WNZ exhibited few but large and deep pits (black in color). Surface roughness of corroded specimens of WNZ (570.24 nm) and base metal (349.63 nm) was found higher than un-corroded specimen (265.1 nm). These results are in accordance to results obtained from Tafel analysis which showed higher current density i.e. corrosion rate for WNZ consequently poor surface finish of the same.

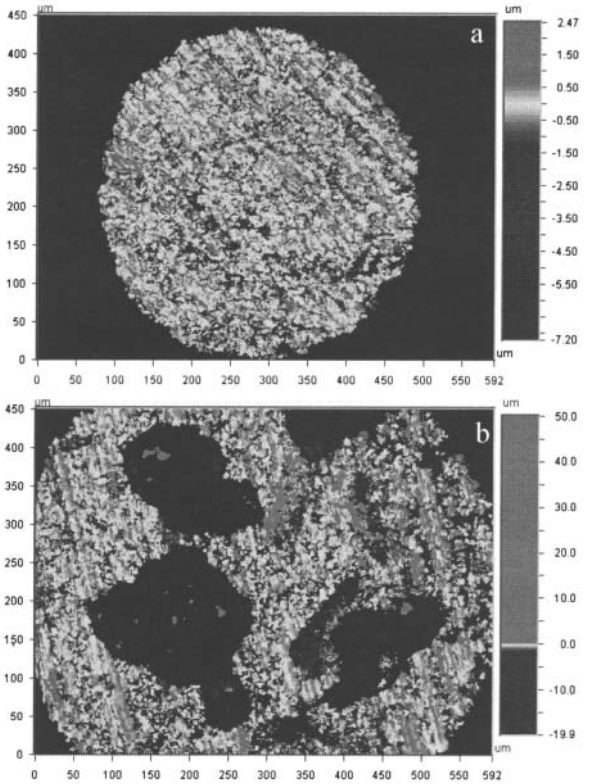


**Fig.5: Surface roughness plots for a) base metal, and b) WNZ**

## 7. Conclusions

Al alloy AA7039 is readily weldable by FSW. The % elongation of FSW joints was higher (41.7%) than base metal. The yield strength and ultimate tensile strength of the joint was 66.3 and 85.6% lower than that of base metal. Fracture of FSW joints took place from minimum hardness region of HAZ on AS. The fracture surface of FSW joint was mostly ductile. WNZ and HAZ of FSW joints showed lower corrosion resistant than base metal. The current density for WNZ and HAZ were ~8.5 and 2.8 times higher than that of the base metal resulting in higher corrosion rates. WNZ and HAZ had increased anodic reactivity than base metal.

## References


1. Hassan Kh. AA., Prangnell P.B., Norman A.F., Price D.A., Williams S.W. Effect of welding parameters on nugget zone microstructure & properties in high strength Al alloy FS welds. Scie. & Tech. of Weld. & Join. 2003, 8(4): 257–268.
2. Rhodes CG, Mahoney MW, Bingel WH. Effects of FSW on microstructure of 7075 Al. Scripta Materilia 1997, 36:69–75.
3. Threadgill et al. FSW of aluminium alloys. International Materials Reviews 2009, 54 (2): 49-93.
4. ASM Handbook Volume 2, Properties and Selection: Nonferrous Alloys and Special-Purpose materials. ASM international material park,USA 1992
5. C. S. Paglia and R. G. Buchheit, A look in the corrosion of Al alloy FS welds. Scripta Materialia2008, 58: 383–38.

6. P. S. Pao, S. J. Gill, C. R. Feng and K. K. Sankaran, Corrosion fatigue crack growth in friction stir welded 7050 aluminium alloy. Scripta Materialia 2001, 45: 605-612.
7. Colligan K. Material flow behaviour during friction welding of aluminum. Welding Journal 1999, 229s-237s.
8. Zhang Z., Zhang H.W. Numerical studies on controlling of process parameters in friction stir welding. Journal of Materials Processing Technology 2009, 209: 241–270.
9. Mahoney M.W., Rhodes C.G., Flintoff J.G., Spurling R.A, Bingel W.H. Properties of FSWed 7075 T651 Al. Metallurgical & Materials Transaons A 1998, 29 A: 1955-64.
10. Liu H.J., Fujii H., Maedaa M., Nogi K. Tensile properties & fracture locations of FSWed joints of 2017-T351 Al alloy. Journal of Materials Processing Techn. 2003, 142: 692–696.
11. Cavaliere P., Squillace A., Panella F. Effect of welding parameters on mechanical and microstructural properties of AA6082 joints produced by friction stir welding. Journal of Materials Processing Technology 2008, 200: 364–372.
12. Kumar K., Satish V. Kailash. On the role of axial load and effect of interface position on the tensile strength of a FSwed Al alloy. Materials and Design 2008, 29: 791-797.
13. M. Jariyaboon, A. J. Davenport, R. Ambat, B. J. Connolly, S. W. Williams and D. A. Price, The effect of cryogenic $CO_2$ cooling on corrosion behaviour of FSwed AA2024-T351. Corrosion Engg. Science & Techno 2009, 44 (6), 425-32.
14. Balasubbramanian V. Relationship between base metal properties and friction stir welding process parameters. Materials science and engineering A 2008; 480:397-403.
15. Singh R.K.R., Sharma Chaitanya, Dwivedi D.K., Mehta N.K., Kumar P. The microstructure and mechanical properties of FSWed Al–Zn–Mg alloy in as welded and heat treated conditions. Materials and Design 2011, 32: 682–687.
16. ASTM E8/E8M-09. Standard test methods for tension testing of metallic materials. ASTM International, USA, December 2009.
17. Cabibbo M., McQueen H.J., Evangelista E., Spigarelli S., Di Paola M., A Falchero. Microstructure and mechanical property studies of AA6056 FSWed plate. Journal of Material Science and Engineering A 2007, 460-461: 86-94.
18. Chen Y., Liu H., and Feng J. Friction stir welding characteristics of different heat treated state 2219 Al alloy plates. Material Science & Engineering A 2006, 420:21-25.
19. ASM Handbook Volume 13A, Corrosion: Fundamentals, Testing, and Protection. ASM international material park,USA.
20. Venugopal T., K.S. Rao, and K. P. Rao. Studies on FSWed 7075 al alloy. Trans. Indian Inst. Met. 2004, 57(6): 659-663.
21. M. Jariyaboon, A. J. Davenport, R. Ambat, B. J. Connolly, S. W. Williams and D. A. Price, The effect of cryogenic cooling on corrosion of FSwed AA7010-T7651. Anti Corrosion Methods and Materials 2010, 57(2): 83-89.

**Table 3: Mechanical properties of FSW joints of AA7039**

| Material Condition | Yield Strength (MPa) | Ultimate Tensile Strength (MPa) | Elongation (%) | Energy Absorbed (J) | Strength Efficiency (%) | Elongation Efficiency (%) |
|---|---|---|---|---|---|---|
| Base metal | 328 | 414 | 15.1 | 15.1 | - | - |
| As welded joint | 217.3 | 354.4 | 21.4 | 18.7 | **85.6** | **141.7** |

**Table 4: Corrosion properties of base metal, WNZ and HAZ**

| Alloy condition | OCP (mV vs. Ag/AgCl)) | Corrosion potential $E_{corr}$ (mV vs. Ag/AgCl) | Current density $I_{corr}$ ( $\mu A/cm^2$) |
|---|---|---|---|
| **Base metal** | -929.3 | -922.44 | 1.168 |
| **WNZ** | -949.3 | -938.46 | 9.834 |
| **HAZ** | -951.9 | -943.71 | 3.277 |